J. ENVIRONMENTAL SYSTEMS, Vol. 33(1) 29-55, 2011

A CFD MODEL FOR SIMULATING AREA SOURCE POLLUTANT DISPERSION IN URBAN CANYON*

PENG WANG
Guangzhou Institute of Energy Conversion
Chinese Academy of Sciences, China

ABSTRACT

In this article, the urban canyon flow and dispersion field, turbulent kinetic energy field and pollutant concentration field are obtained by a three-dimensional computational fluid dynamics (CFD) model. The governing equations are the Reynolds-averaged equations of momentum, mass continuity, heat, and other scalar (here, passive pollutant) under the Boussinesq approximation with k-ε turbulent model. The concentration field in different layers of three planes was examined through making slices of flow field and streamline field. Through the analysis of the wind speed profile, turbulent kinetic energy profile and wind direction profile at the position of upwind, downwind, and middle canyon, some useful results were obtained. The simulation results were compared with the available wind tunnel experiments (Meroney et al., 1996) and favorable agreement between them was found.

1. INTRODUCTION

Harmful pollutants emitted from traffic vehicles in an urban area cause serious damages to human health. In order to minimize potential damage incurred by human activity, it is demanded not only to reduce emissions of harmful pollutants but also to understand and accurately predict urban flow and pollutant dispersion.

*This work is supported by Director Innovation Fund of Chinese Academy of Sciences under the contract No. Y007R81001.

doi: 10.2190/ES.33.1.c
http://baywood.com

An urban street canyon is a space surrounded by a city road and its flanking buildings and a main pollutant-emitting source, traffic vehicles, is located at the street. Therefore, a study of flow and pollutant dispersion in an urban street canyon should be a first step to understand complex urban flow and dispersion (Kim & Baik, 2003).

Flow and dispersion in urban canopy are very complicated because of complex building configurations and ever-changing meteorological conditions. Extensive studies on the flow and dispersion in urban canopy have been conducted to improve our understanding on fluid dynamical processes, accurately predict them and minimize the damage caused by harmful pollutants, and help urban planners to take into account urban geometry with optimal natural ventilation and comfort. These studies include the investigations of flow regimes (Chan, Dong, Leung, Cheung, & Hung, 2002; Sahm, Louka, Ketzel, Guillouteau, & Sini, 2003; Assimakopoulos, Apsimon, & Moussiopoulos, 2003; Koutsourakis, Neofyton, Venetsanos, & Bartzis, 2005) and the researches on the dispersion (e.g., Meroney et al.,1996; Kastner-Klein et al., 2001; Neotytou, Venetsanos, Rafailidis, & Bartzis, 2006) in urban street canyons, thermal effects on urban street-canyon flow and dispersion, and so on. Leitl and Meroney (1997) and Xie, Huang, and Wang (2005) have evaluated the pollutant concentration in two- and three-dimensional urban street canyons using the standard model and the RNG k-ε turbulence model. Hassan and Crowther (1998) and Koutsourakis et al. (2005) reported a series of simulation for transport and dispersion processes of pollutants in urban street canyons with different wind speed and canyon configurations. Ahmadi and Li (2000) have simulated the flow and particulate pollutant transport near an isolated building using a Lagrangian particle tracking method. Chan, Au, and So (2003) studied the flow field and pollutant dispersion characteristics in a three-dimensional urban street canyon formed by a multi-canopy building using a computational fluid dynamics (CFD) in conjunction with k-ε turbulence model. Neofytou et al. (2006) investigated the pollution levels in a real urban street canyon using the Reynolds averaged Navier-Stokes (RANS) equations under realistic conditions. Baik, Kang, and Kim (2007) examined reactive pollutant dispersion in an urban street with a street aspect ratio of one using a CFD model incorporated by a simple NO-NO2-O3 photochemistry and Ryu and Baik (2009) examined the flow and dispersion in an urban cubical cavity. Yassin et al. (2009) studied the impact of street intersections on the air quality in an urban environment.

Despite of our understanding of the impact factors to pollutant dispersion in street canyons from the previous studies, there appears to be some controversies regarding the process responsible. The accuracy of the previous models on the simulation of pollutants transport from the canyon are limited by the fact that most of them are only two-dimensional. In this work, a three dimensional numerical model was developed to investigate the pollutant dispersion mechanism and general guidelines in promoting better circulation patterns in

real-life situations. This study aims at investigating the three-dimensional flow field and dynamical processes of these problems through numerical model simulations. However, despite the common employment of Computational Fluid Dynamic technique, the use of the k-ε turbulence closure model does not always guarantee a successful prediction of the real canyon situation. The results and guidelines reported here are designed to provide an initiative idea for the future study of a field size three-dimensional canyon problem and help to induct engineering practice or decision support.

The numerical model used in this study is described in Section 1. In Section 2, the numerical model is validated against the data from wind-tunnel experiments. The results associated with pollutant concentration field and the turbulent kinetic energy are presented and discussed in Section 3. Finally, summary and conclusion are given in Section 4.

2. MATERIALS AND METHODS

2.1. Numerical Modeling

The standard k-ε turbulence model represents the effects of turbulence by including two more variables: namely, the turbulent kinetic energy, TKE, and its dissipation rate. Those two quantities are treated as variables in transport equations, which have to be solved together with the usual Reynolds-averaged Navier-Stokes equations, involving continuity and momentum conservation. The conservation equation for the concentration of pollutants must also be solved together with the above-mentioned equations which describe the flow characteristics.

The governing equations of the model are shown below.

Continuity equation:

$$\frac{\partial u_i}{\partial x_i} = 0 \tag{1}$$

Momentum equation:

$$\frac{\partial u_i}{\partial t} + \frac{\partial}{\partial x_j}(u_j u_i) = -\frac{1}{\rho \partial x_i}\frac{\partial p}{\partial x_i} + \frac{\partial}{\partial x_i}\left\{ v\left(\frac{\partial u_i}{\partial x_j} + \frac{\partial u_j}{\partial x_i} \right) - \overline{u_i' u_j'} \right\} \tag{2}$$

TKE transport equation:

$$\frac{\partial k}{\partial t} + \frac{\partial k u_i}{\partial x_i} = \frac{\partial}{\partial x_i}\left(\frac{v_t}{\sigma_k}\frac{\partial k}{\partial x_i} \right) + v_t\left(\frac{\partial u_i}{\partial x_j} + \frac{\partial u_j}{\partial x_i} \right)\frac{\partial u_i}{\partial x_j} - \varepsilon \tag{3}$$

ε transport equation:

$$\frac{\partial \varepsilon}{\partial t}+\frac{\partial \varepsilon u_i}{\partial x_i}=\frac{\partial}{\partial x_i}\left(\frac{v_t}{\sigma_\varepsilon}\frac{\partial \varepsilon}{\partial x_i}\right)+c_{1\varepsilon}\frac{\varepsilon}{k}v_t\left(\frac{\partial u_i}{\partial x_j}+\frac{\partial u_j}{\partial x_i}\right)\frac{\partial u_i}{\partial x_j}-c_{2\varepsilon}\frac{\varepsilon^2}{k} \quad (4)$$

Species transport equation:

$$\frac{\partial c}{\partial t}+\frac{\partial u_j c}{\partial x_j}=\frac{\partial}{\partial x_j}\left(D\frac{\partial c}{\partial x_j}-\overline{c'u'_j}\right)+S_c \quad (5)$$

$$-\overline{u'_i u'_j}=v_t\left(\frac{\partial u_i}{\partial x_j}+\frac{\partial u_j}{\partial x_i}\right)-\frac{2}{3}k\delta_{ij} \quad (6)$$

$$-\overline{c' u'_j}=v_c\frac{\partial c}{\partial x_j} \quad (7)$$

$$v_t=c_\mu\frac{k^2}{\varepsilon} \quad (8)$$

$$Sc_t=\frac{v_t}{v_c} \quad (9)$$

where u_i is the ith mean velocity component, p is the deviation of pressure from its reference value, c is the mean concentration of any passive scalar (i.e., any pollutant), u_0 and c_0 are fluctuations from their u_i and c, respectively and ρ is the air density. v_t and v_c are the turbulent viscosities of momentum and pollutant concentration, respectively, S_{ct} is the turbulent Schmidt number, δ_{ij} is the kronecker delta. v is the kinematic viscosity of air, D is the molecular diffusivity of pollutant, S_c denotes the source of pollutant. Cμ = 0.09, σ*k*= 1.0, σε = 1.3, $C_{1\varepsilon}$ = 1.44, $C_{2\varepsilon}$ = 1.92, and S_{ct} = 0.9.

2.2. Model Domain and Meshing

The idealized street canyon in the Fluent model comprised two buildings with height H, width B, and Length L, separated by a street width of W, illustrated in Figure 1. The origin of the coordinate system is located at the left side of the street bottom in the computational domain. The domain size is 180 m in the x-direction, 150 m in the y-direction (L), and 100 m in the z-direction. The building height H is 40 m and the width between two buildings W is 40 m, giving a street aspect ratio of one.

The initial wind direction above the canyon was in the x-direction perpendicular to the street axis, which lies along the y-axis, while the z-axis corresponds

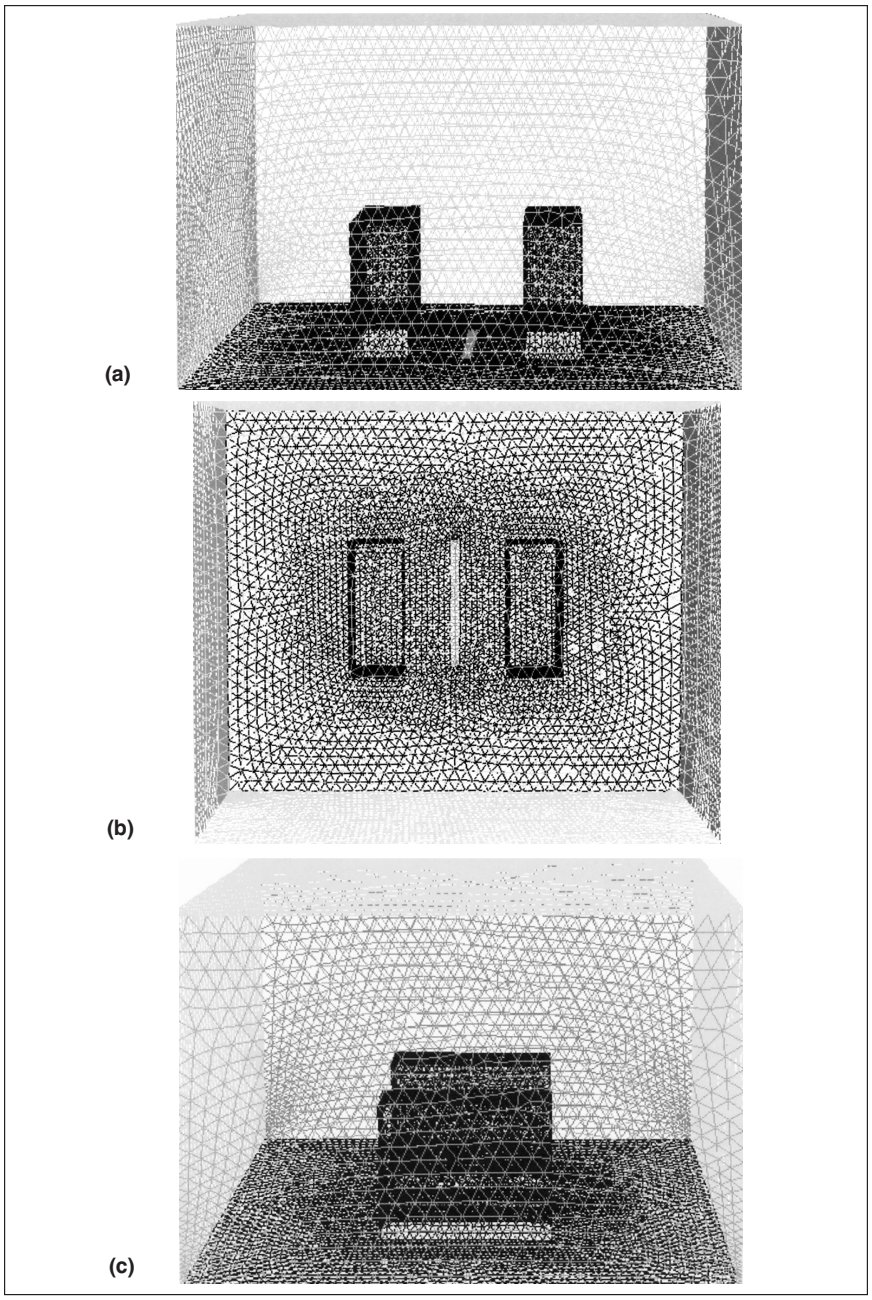

Figure 1. Schematic canyon model and computational grid
(a) x-z plane, (b) x-y plane, (c) y-z plane.

to the vertical. Inlet and Outflow boundary conditions were specified for wind components in the y-z plane. A zero normal velocity component boundary condition (i.e., no airflow out of the domain top), can be established at the top of the domain, over five times the canyon top height.

This study models area sources pollutant dispersion in a long street canyon when the ambient wind direction (x-direction) is perpendicular to the along-canyon direction (y-direction). The grid intervals counts are uniform in the horizontal with 40 and 40 count numbers of unstructured grids. In the vertical, the grid interval increases with an expansion ratio of 1.1. The model is integrated for steady state until 360 times convergence.

2.3. Boundary Conditions

Velocity inlet boundary layer conditions were used in the main inlet wind flow and the vehicle exhaust. The initial wind speed is 1.5 m/s in 10 m height with low turbulence intensity. A user-defined subroutine for including the turbulence 0.28 of the power law inlet velocity profile into FLUENT code was developed and used in the analysis. The initial condition for wind velocities, turbulent kinetic energy (TKE), and its dissipation rate e are specified as (FLUENT, 2005).

$$U = U_0 \left(\frac{Z}{Z_H} \right)^n \tag{10}$$

$$T_{KE} = \frac{u_\tau^2}{\sqrt{c_\mu}} \tag{11}$$

$$\varepsilon = \frac{c_\mu^{3/4} (T_{KE}^{3/2})}{l} \tag{12}$$

where U_0 is the velocity at a height Z_0, Z_0 is the height above the ground 10 m, and n is the power exponent, u_τ is the friction velocity and l is the turbulence length scale. The ground and building surfaces are defined as walls with no-slip boundary condition. The wall boundary conditions for momentum are applied to all solid surface and rough walls. Zero gradient boundary conditions are applied at the outflow and upper boundaries. C_μ is a const equals 0.09.

3. MODEL VALIDATION

To assess the accuracy of the present computer simulation procedure, the three-dimensional CFD model with the standard k-ε turbulence scheme is validated against the wind tunnel data of Meroney et al. (1996). Meroney et al. (1996) performed a series of wind tunnel experiments for a model of two isolated

buildings in an open space. In the experiment, the building height was 6 cm and the street width was varied from 6 to 48 cm, and the study was performed for a range of wind speeds from 0.5 to 10 m/s. Ethane was used as a model pollutant and was emitted from the center of the street in the model.

The building configuration follows a 2-D array of buildings. The ambient wind direction is perpendicular to the building. The simulated data are interpolated at the same grid points in the wind tunnel experiment. The results are presented in Figure 2.

Meroney et al. (1996) presented their measured pollutant concentrations in terms of a dimensionless concentration parameter, *K,* which is defined as

$$K = \frac{CU_{\infty} h}{Q_{Poll} / \ell} \tag{13}$$

Here, C is volume fraction of the pollutant (CO2 in our study), U_{∞} is the free stream velocity, h is the building height, and Q_{Poll}/ℓ is the emission source strength per unit width. To test the accuracy of different turbulence models, the computations were repeated using the standard k-ε and the Realizable k-ε

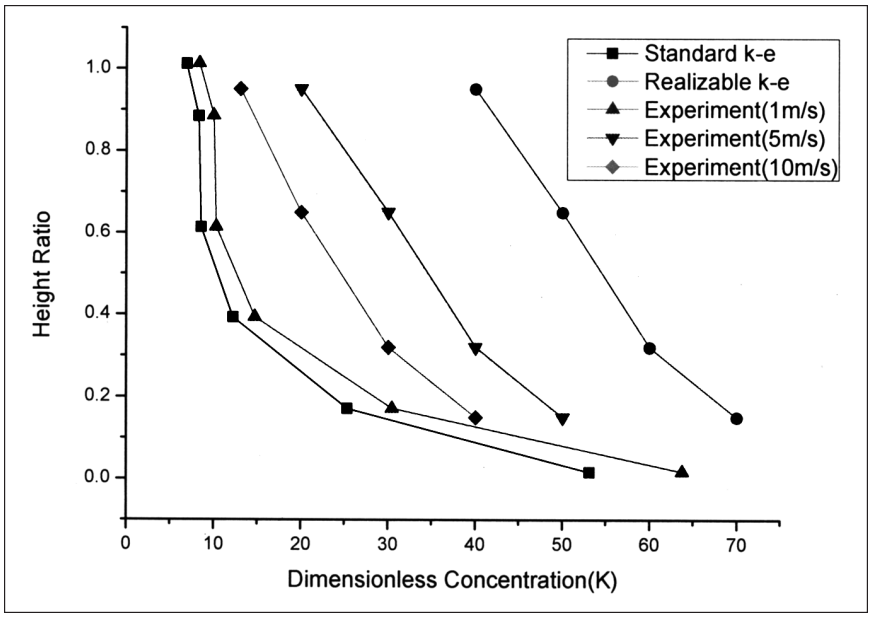

Figure 2. Comparison of dimensionless concentration along the leeward wall as predicted by different turbulence models with wind tunnel experiment of Meroney et al. (1996).

models as well. The resulting pollutant concentration contours were evaluated. In all cases, it was assumed that CO2 gas enters the street with volumetric flux of 4 liter/h from the middle of the street at the experiments of Meroney et al. (1996).

3.1. Velocity Field Validation

The inflow is parallel to the upwind-building top surface, and no flow separation is observed. However, flow separation is observed at the upwind edge of the downwind building (Figure 3).

Figure 3 shows the simulated fields of velocity vector (U, W) and velocity vector (U, V) on the x-z plane at y = 60 m and on the x-y plane at z = 20 m. One vortex is formed in the street canyon. The center of the canyon vortex is slightly shifted down-wind and upward (x = 90 m, z = 45 m) from the canyon center (x = 90 m, z = 20 m).

3.2. Concentration Field Validation

Although the dimensionless concentration is underestimated to some extent in the leeward wall of the street canyon (see Figure 2), the main features of the mean flow (roll-type vortices in front of the first building and in the street canyons and recirculation above the first building roof) are simulated well (Figures 3 and 4). The maximum concentration at each position appears in the leeward wall of the street canyon in the experiments, but the numerical model underestimates it at most heights (Figures 5 and 6). Figure 6 shows the simulated fields of pollutant concentration on the x-z plane at y = 100 m and y = 90 m.

It is seen that along the leeward wall, the dimensionless concentration K decreases toward the height of roof level. Figures 6 and 7 also show that the model predictions are in general agreement with the experimental data, but there are some quantitative differences.

Figures 6 and 7 compare the measured values of dimensionless concentration K of Meroney et al. (1996) with the simulated values for the leeward and windward wall of the laboratory model. As the wind speed increases, an increase in the simulated value of K is observed. The predicted non-dimensional concentrations for the physical model are generally lower than that for wind tunnel model. The observed differences could be due to the effects of the bottom surface with large resistance. An agreement between the numerical and wind tunnel experiment as shown in Figure 2 will reliably support the physical realism of numerical model results presented in the next section.

4. SIMULATION RESULTS AND ANALYSIS

The governing equation set is numerically solved on a staggered grid system using a finite-volume method with the semi-implicit method for pressure-linked equation (SIMPLE) algorithm (Patankar, 1980). To test the CFD model described

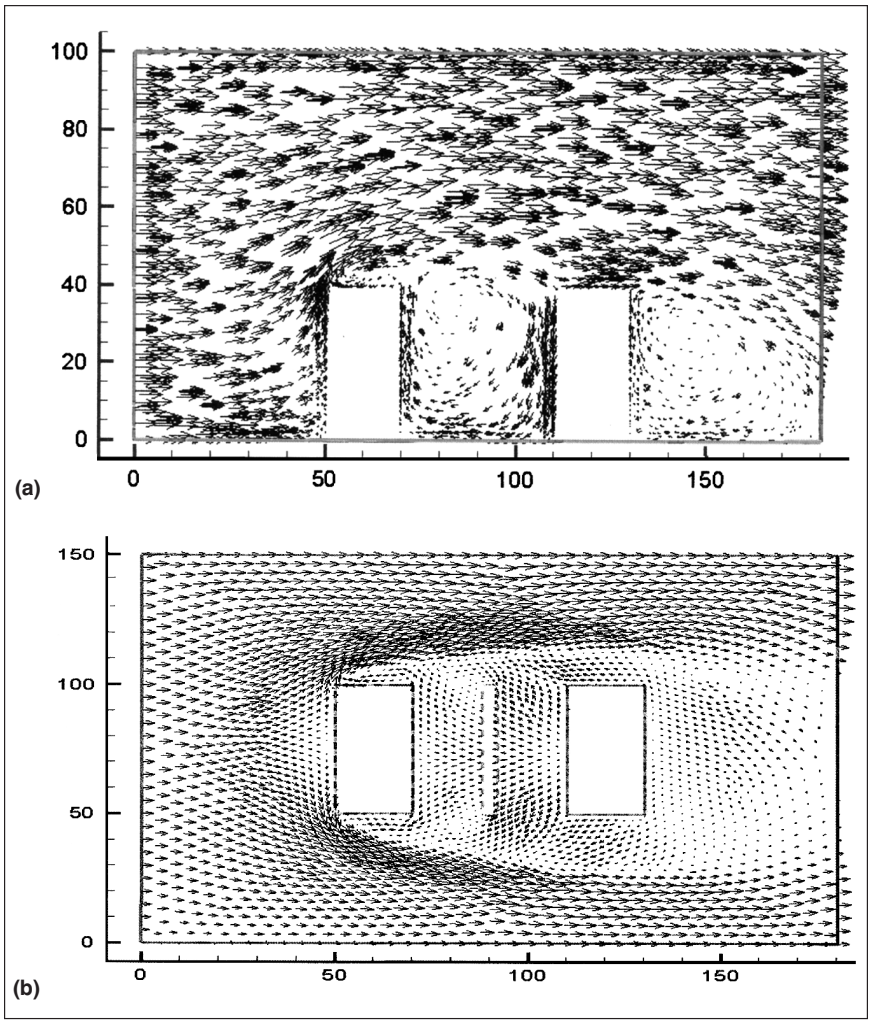

Figure 3. Velocity vector field using standard k-ε model
(a) x-z plane y = 60 m, (b) x-y plane z = 20 m.

in section 1 and to understand basic fluid dynamics associated with urban street-canyon flow and dispersion, the three-dimensional characteristics of flow in the canyon are examined first.

4.1. Streamline Analysis

The fields of mean flow within the street canyon are presented in x-z plane at y = 55 m, y-z plane at x = 110 m and x-y plane at z = 14 m, through making a

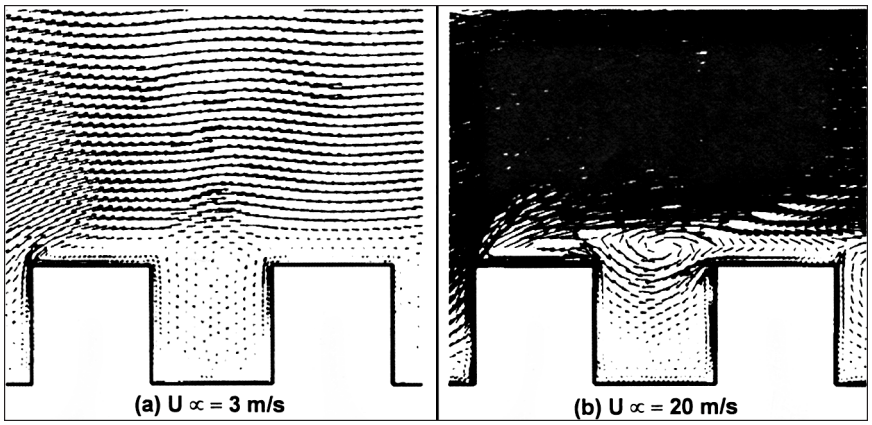

Figure 4. Velocity vector field for the wind tunnel model in Meroney et al. (1996).

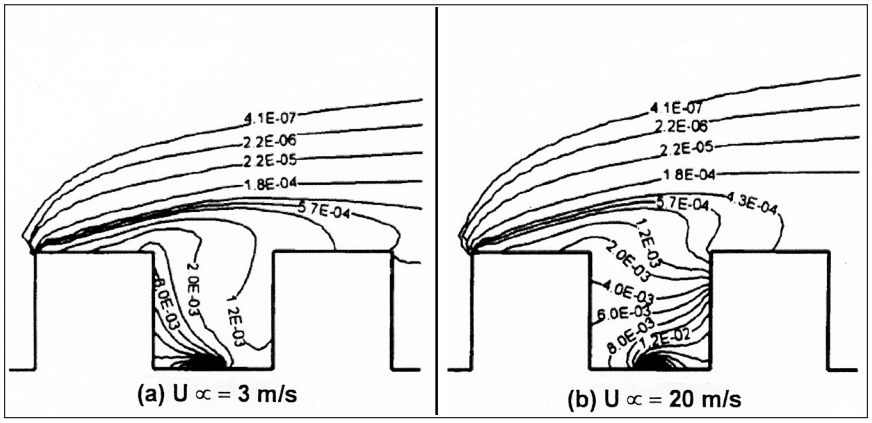

Figure 5. CO2 mass fraction for the wind tunnel model in Meroney et al. (1996).

slice from the three-dimensional simulation field. Figure 7 shows streamline fields at different planes of (a) x-z plane y = 55 m, (b) y-z plane x = 110 m, (c) x-y plane z = 14 m. The streamline field in Figure 7(a) shows a well-organized, clockwise-rotating vortex within the canyon. The primary vortex is produced in the canyon and upstream and downstream vortices appear at the bottom corners

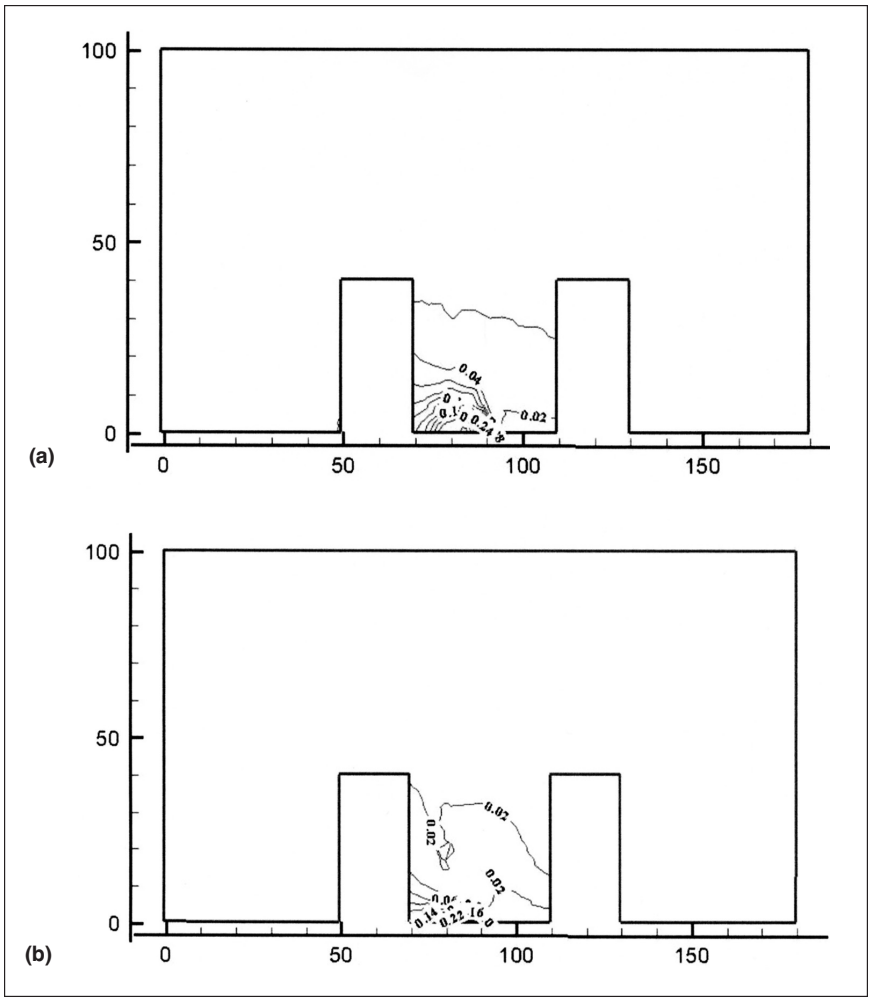

Figure 6. CO2 mass fraction contours
(a) x-z plane y = 100 m, (b) x-z plane y = 90 m.

of the canyon in Figure 7(a). These flow patterns in the x-z plane are similar to those in an urban street canyon studied by Kim and Baik (2003).

However, flow patterns represented in the x-y and y-z planes in Figures 7(b) and 7(c) are quite different from those in a two-dimensional street canyon model because of the not infinite long street canyon in spanwise direction. Figure 7(b) shows that there exists two vortices on both sides of the canyon in the y-z plane. We found that along the spanwise direction, the velocity field on the y-z plane

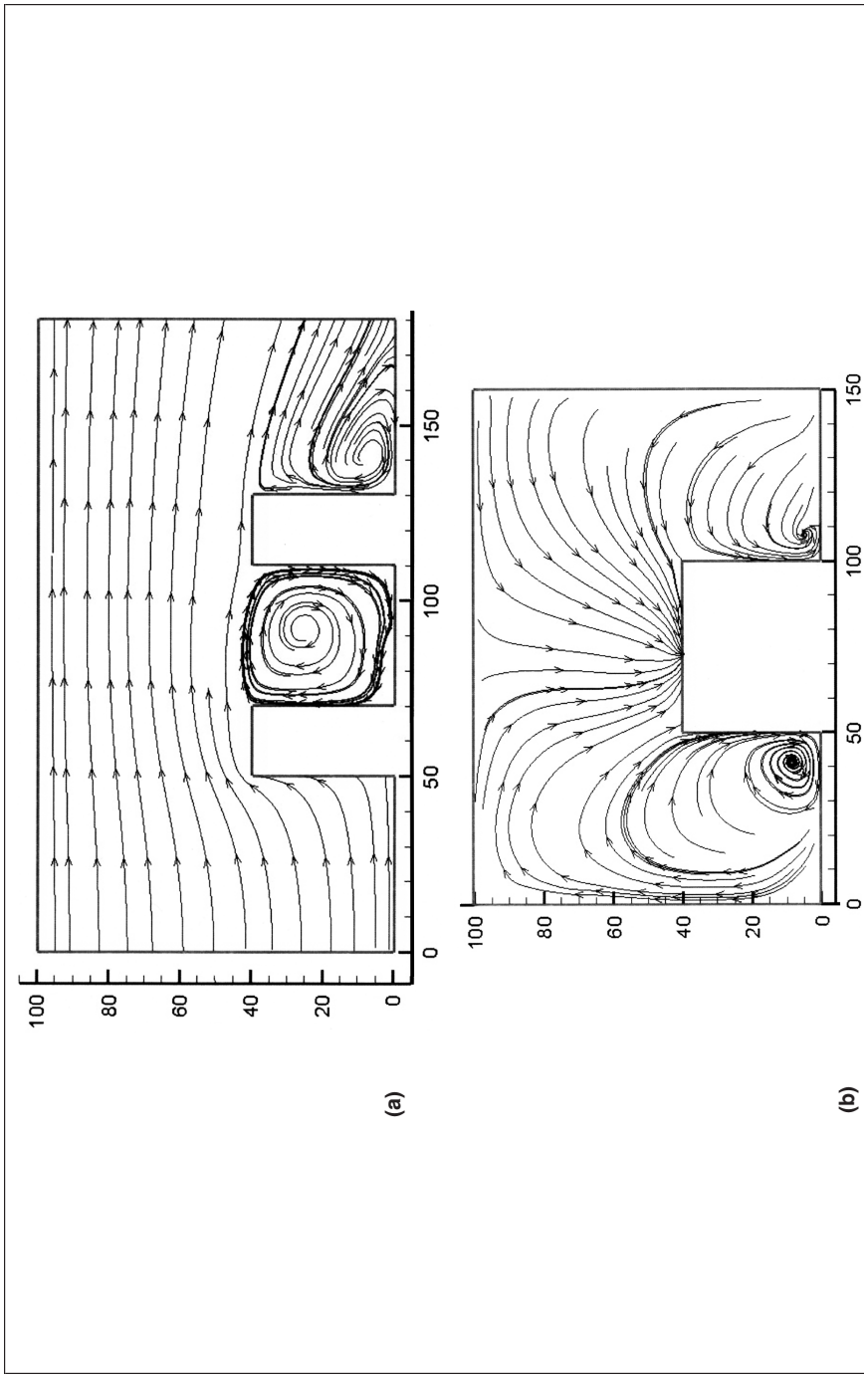
0
50
100
150
0
20
40
60
80
100
(a)
(b)

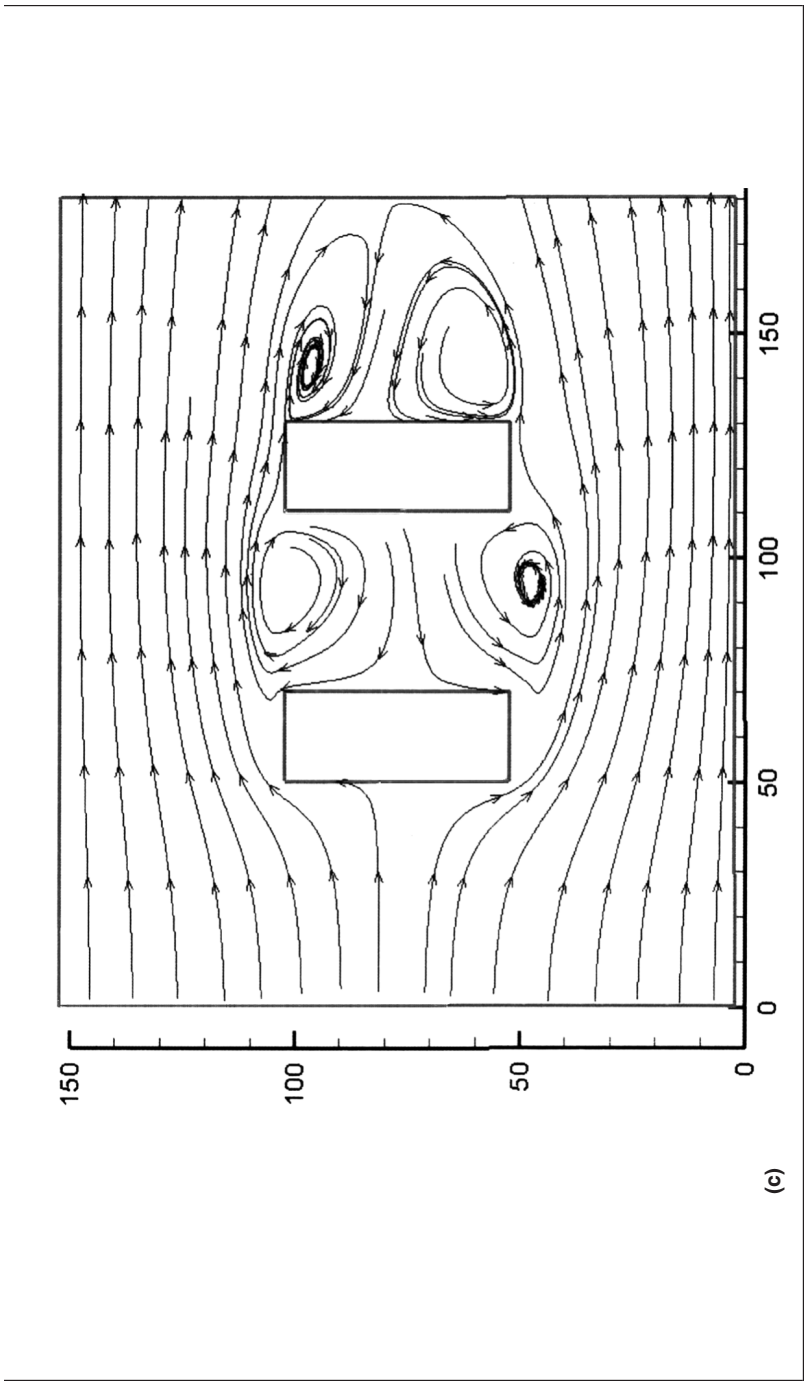

Figure 7. Streamline field (a) x-z plane y = 55 m, (b) y-z plane x = 110 m, (c) x-y lane z = 14 m.

remains symmetrical in Figure 7(b). This result indicates that our CFD model successfully simulates two symmetrical roll-type vortices in y direction.

When the ambient wind direction is perpendicular to the along-canyon direction, the street canyon flow of this model is essentially not two-dimensional and there is very much variation of flow in the along-canyon direction that impact of the dispersion of the pollutant.

4.2. Analysis of the Pollutant Concentration Field in Different Height in x-y Plane

The pollutant concentration is very high near the source location, from where pollutant is transported toward the upwind building and then upward by the vortex circulation. We establish four x-y plane slices from three dimensional simulation field at the layer of 3 m, 10 m, 18 m, 34 m height, to investigate the concentration field influenced by rotating vortex in different height. Figure 8 shows the CO2 concentration field in x-y plane at z = 3 m, z = 10 m, z = 18 m, and z = 34 m.

From Figure 8 we can obtain that the pollutant concentration distribution is the same at different heights and the pollutant concentration was decreased from bottom to top, and the highest concentration was found in the corner of the upwind building. At any height of the street canyon, the pollutant concentration is higher near the upwind building than near the downwind building. The clockwise vortex circulation was generated in the street canyon when wind flow was blown across the street canyon from the upwind building to the downwind building. The pollutant was carried to the upwind side from the area source and dispersed further in the street canyon as the transport of the vortex. The pollutant concentration on the upwind side was higher than that on the downwind side at the lower region of the street canyon.

This is because the horizontal velocity of the lower region near the downwind building in street canyon was negative, where the vortex was clockwise. As the rotating velocity was small at the lower region of street canyon, it was very difficult to remove the pollutant discharged from the area source out of the street canyon. On the other hand, the mean horizontal velocity of the upper region of street canyon was positive and had a larger rotating velocity. Hence, it could transport the pollutant out of the canyon from downwind side of the buildings. For this reason, the pollutant concentration at the upwind side was higher than that at the downwind side on the higher region of street canyon.

This pattern is because highly polluted air passing through the street canyon is advected upward on the upwind side while relatively less polluted air enters the street canyon by the downward motion on the downwind side. Under these circumstances, pollutant dispersion was solely removed vertically from the

street canyons to the free surface layer by the vertical mean flux and vertical turbulent flux.

4.3. Analysis of Concentration in Different Height in x-z Plane

Figure 9 shows the CO2 concentration field in x-z plane (a) y = 45 m, (b) y = 55 m, (c) y = 65 m, (d) y = 90 m. At the width of 45 m and 90 m of y direction, the concentration distributions are similar and appear larger concentration values as the exist of the two vortex in Figure 7(c). These two symmetric vortex transport the pollutant partly outside the canyon and partly renter in the canyon. As the obstacle of downwind building, there exist two vortexes behind the downwind building. From Figure 8 we find that the pollutant concentration was not transported in the region of downwind building wake as the area source was not strong and the contour value was not presented. If the area source turns intense, the pollutant will be circulated in the wake of the downwind building and appear high concentration that need to be accounted for next research.

4.4. Analysis of Concentration in Different Height in x-y Plane

Figure 10 shows CO2 concentration field in y-z plane at x = 70 m, x = 85 m, x = 90 m, and x = 115 m. Figures 10(a) and 10(d) show the concentration field of the positions at x = 70 m near the upwind building and at x = 115 m near the downwind building in x direction, and the concentration distribution of this two figures are similar. Figures 10(b) and 10(c) show the concentration field of the positions in the middle of the canyon at x = 85 m and x = 90 m, and this two figure distribution is the same. From Figure 10 we can find that the pollutant concentration in middle of the canyon at x = 85 m and 90 m is larger than near the upwind building at x = 70 m and 115 m, as the two vortexes transport and advection of the concentration to the canyon center from Figure 7(c). The concentration of near upwind building and downwind building at x = 85 m and 90 m are larger than the downwind building at x = 115 m, as the pollutant concentration was transported by the primary vortex from downwind to upwind in Figure 7(a).

4.5. Analysis of Velocity Profile and Wind Speed in Different Location

Figure 11 shows the vertical profiles of velocities at x = 25 m, 80 m, and 152 m in the simulation results. The x = 25 wind profiles before upwind building agrees well with the inlet boundary power law wind profile. The x = 80 m and x = 152 m

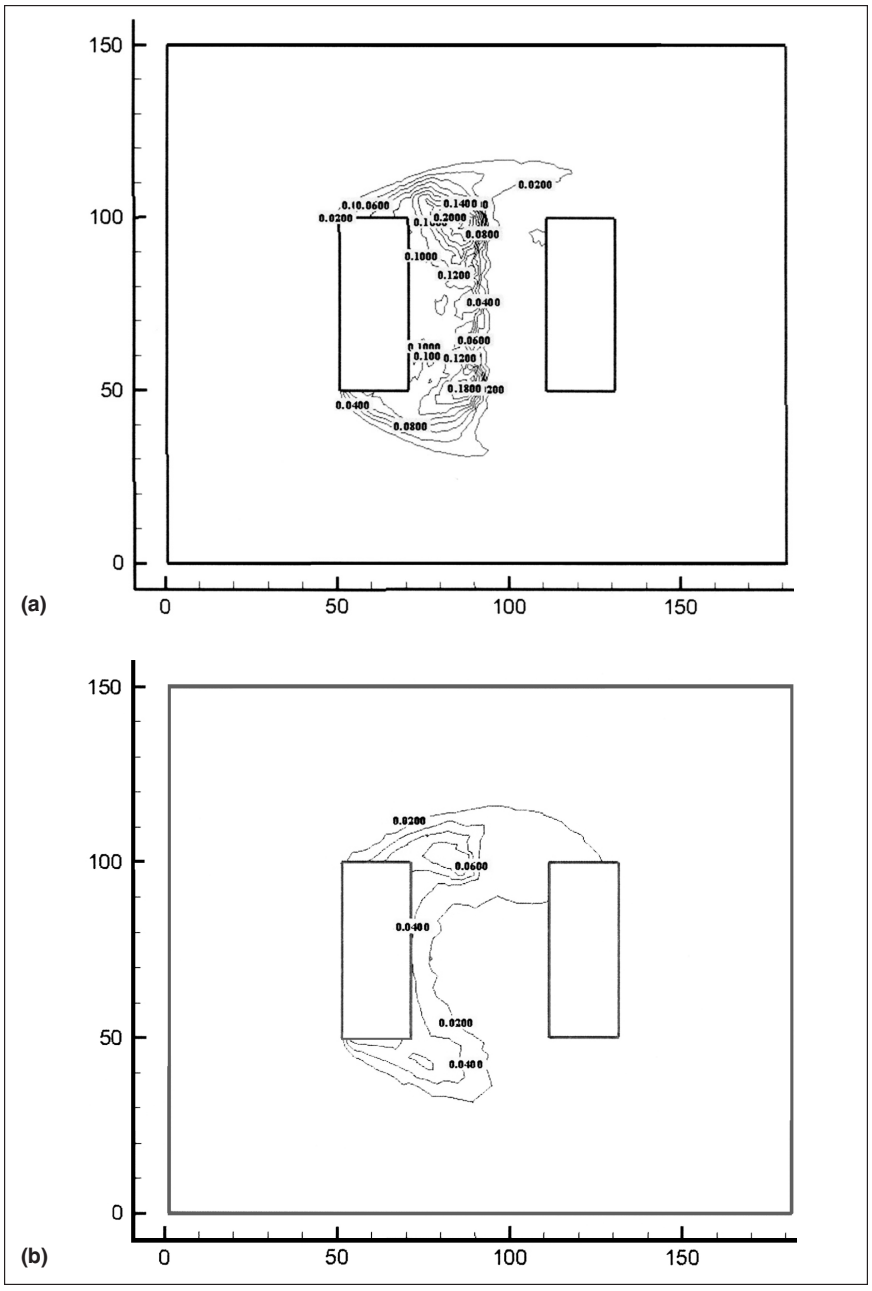

Figure 8. CO2 concentration field in x-y plane
(a) z = 3 m, (b) z = 10 m, (c) z = 18 m, (d) z = 34 m.

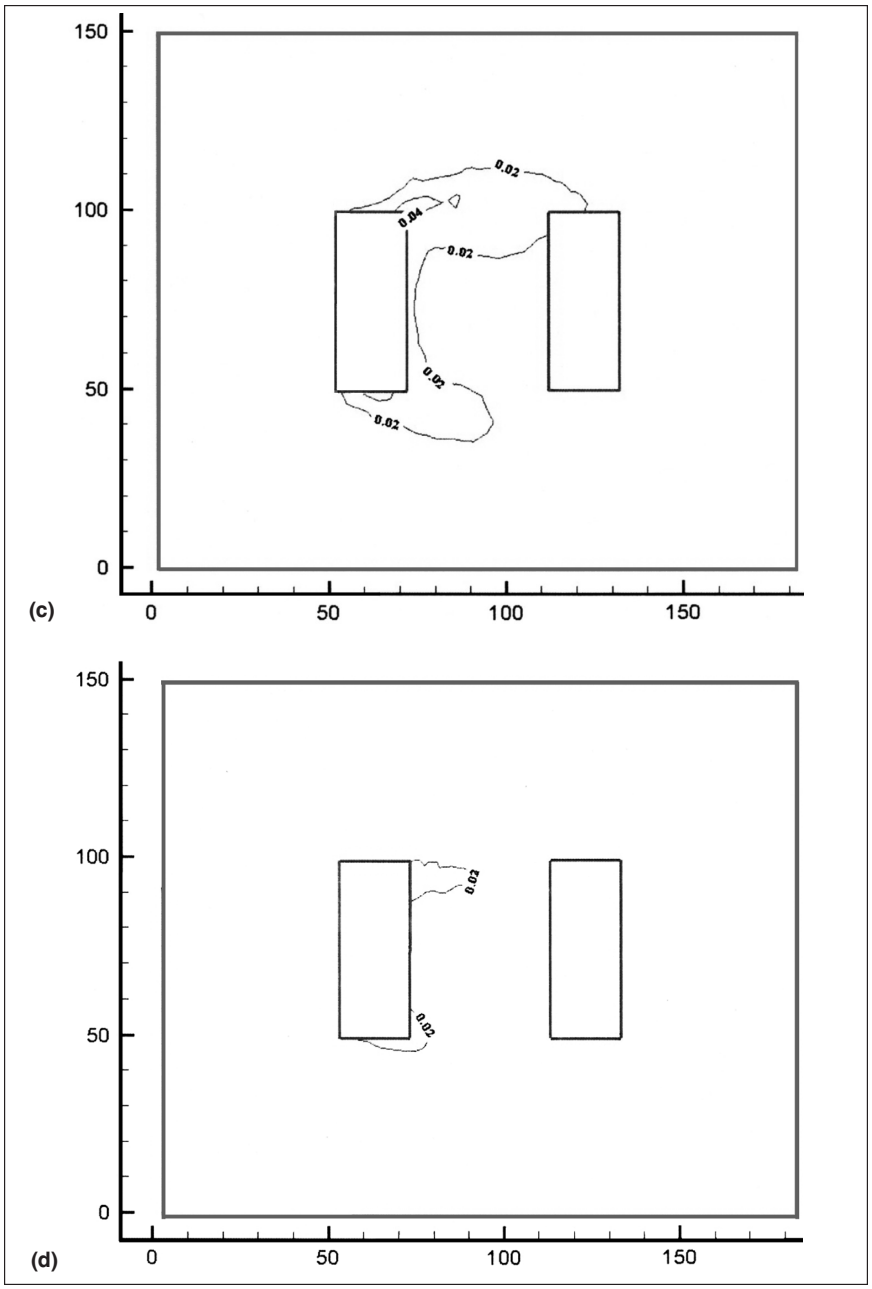

Figure 8. (Cont'd.)

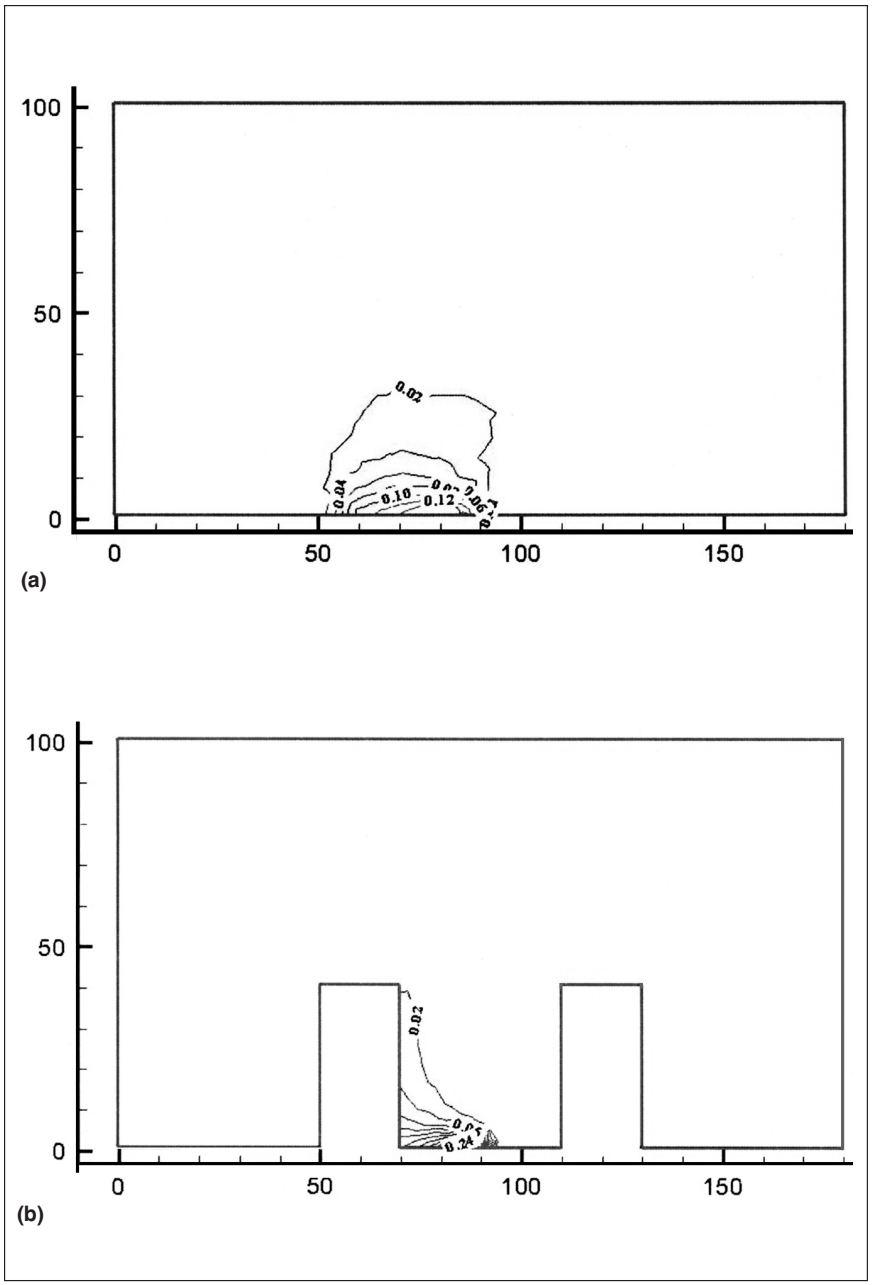

Figure 9. CO2 concentration field in x-z plane (a) y = 45 m, (b) y = 55 m, (c) y = 65 m, (d) y = 90 m.

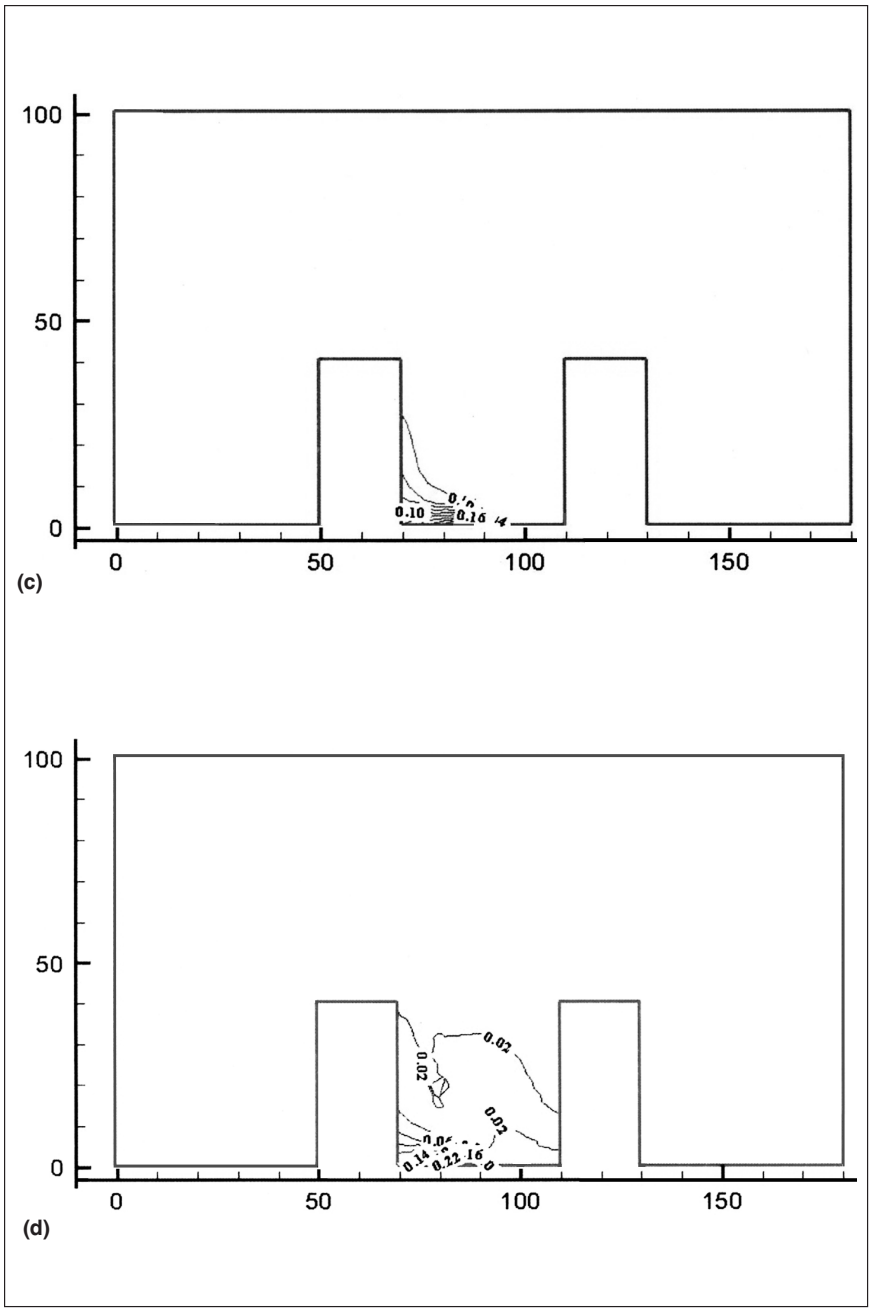

Figure 9. (Cont'd.)

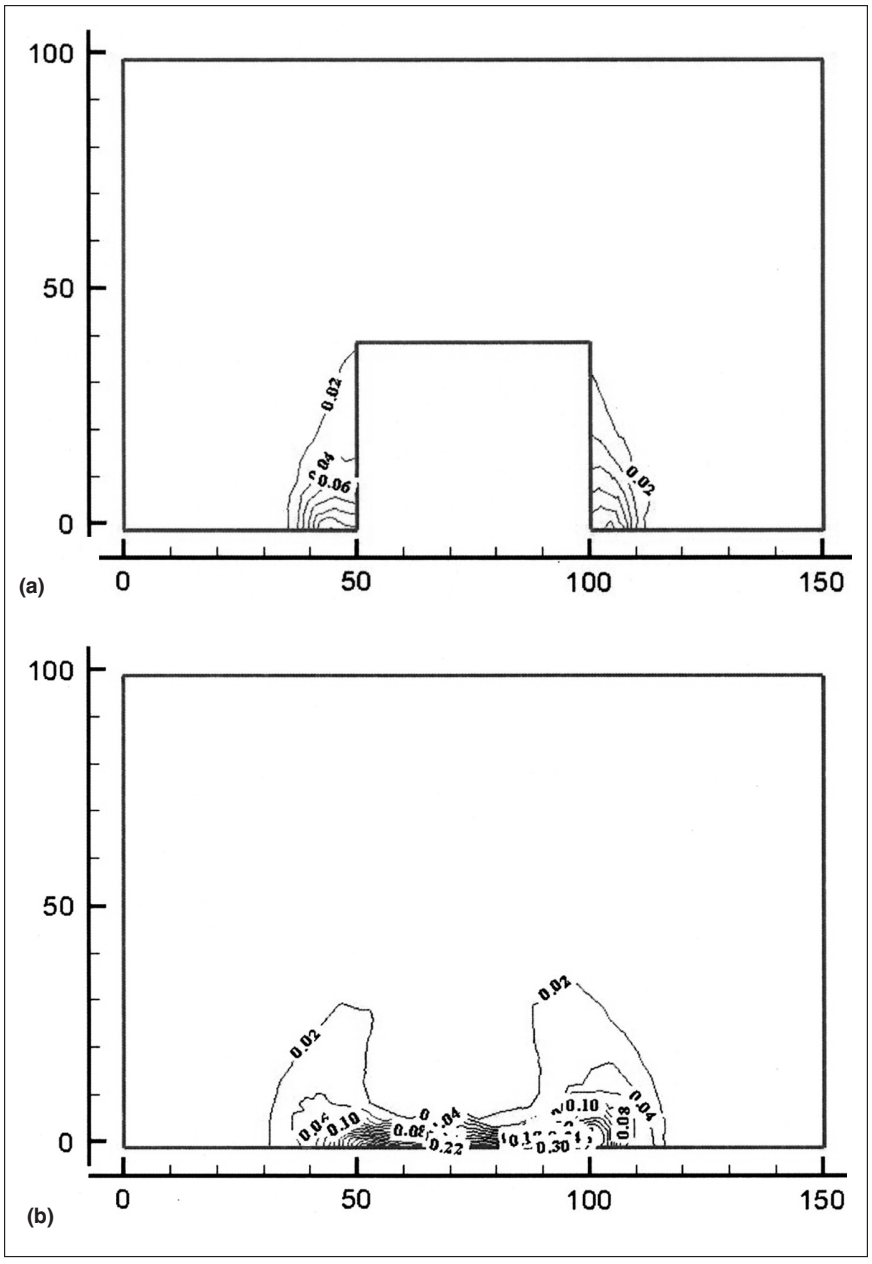

Figure 10. CO2 concentration field in y-z plane (a) x = 70 m, (b) x = 85 m, (c) x = 90 m, (d) x = 115 m.

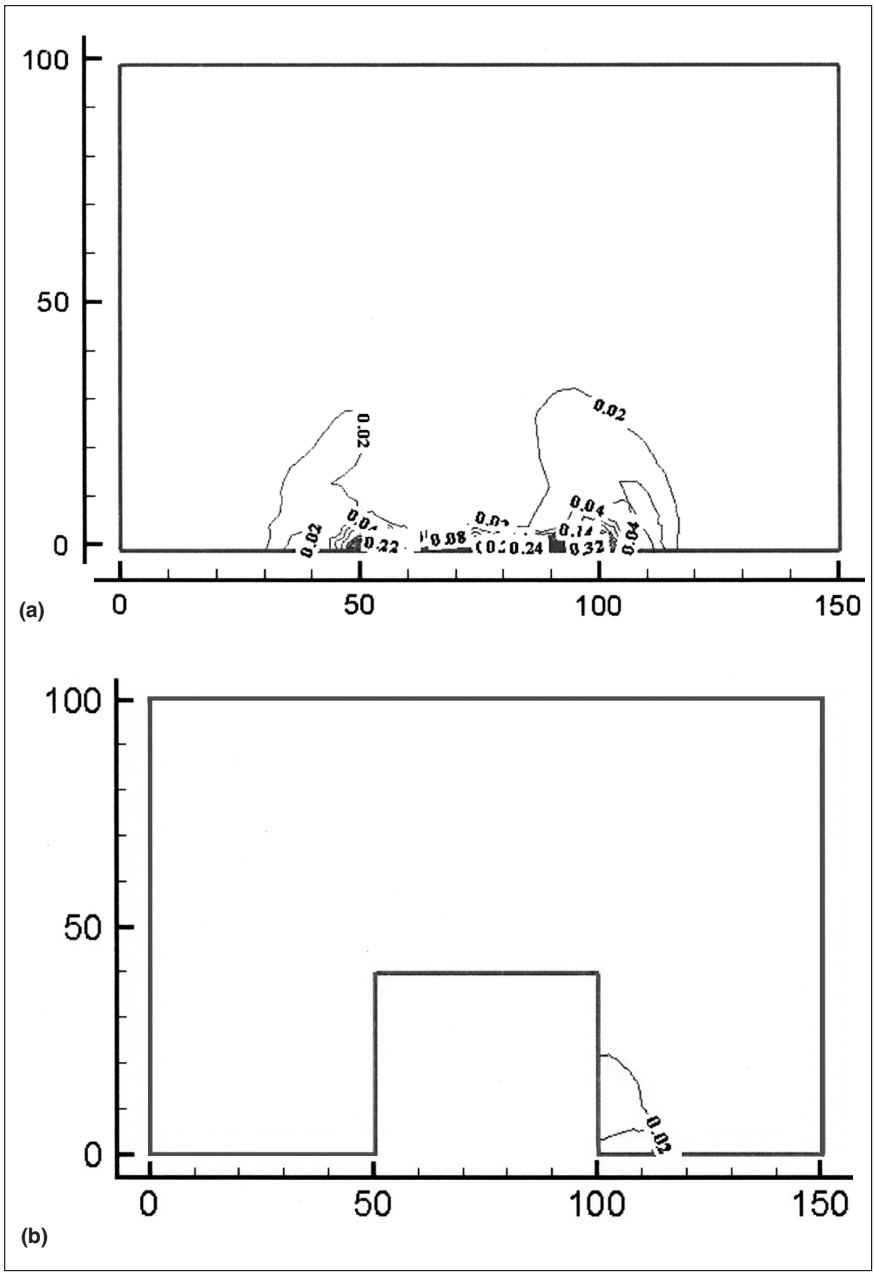

Figure 10. (Cont'd.)

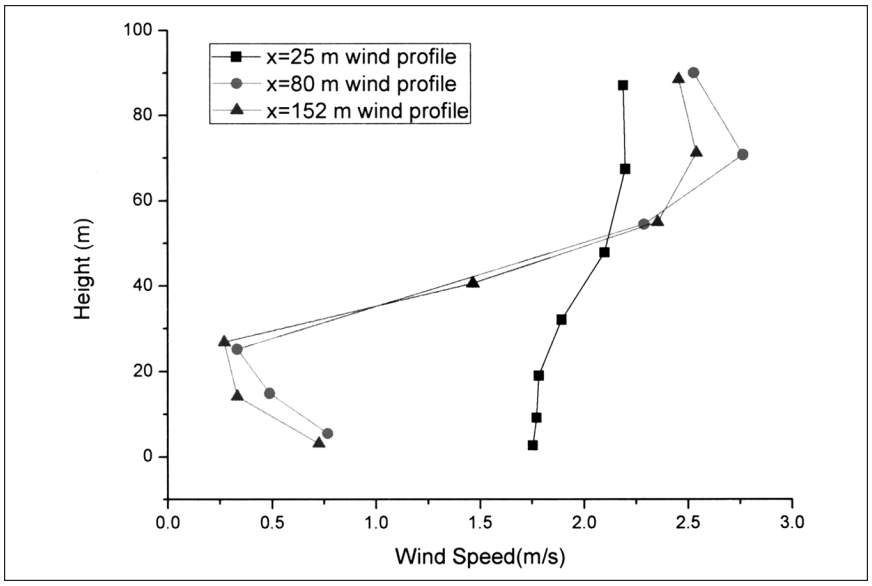

Figure 11. Wind profiles of velocity at x = 25 m, 80 m, and 152 m.

building. The two vertical profiles of the normalized vertical velocity (x = 80 m and 152 m) are closer to each other at the downwind location than the upwind location. The vertical profiles of the velocities at x = 24 m (an upwind location), 80 m (vortex-center location), and 152 m (a downwind location) shown in Figure 11 and 80 m and 152 m profile reflect the circulation of the vortex trapped within the canyon. The velocities at the downwind location (x = 80 m and 152 m) are stronger than that at the upwind location and the velocity of vortex-center location at the downwind location is stronger than the downwind location at the layer of z > 50 m.

At the layer of z < 30 m, the velocity at x = 80 m (vortex-center location), and 152 m (a downwind location) decreases as the increment of height. At the layer of 30 < z < 70 m, the velocity at x = 80 m and 152 m increases as the increment of height and at the layer of z > 70 m, the opposite situation appears. This is because that horizontal velocity is negative in vortex center at x = 80 m and downwind location at x = 152 m produced by the rotating vortex. Within a few meters beneath the roof level namely at the layer of 30 m < Z < 55 m, the horizontal velocity increases with increasing inflow turbulence intensity induced by the roof. At the layer of 55 m < z < 100 m, the impact of increased turbulent kinetic energy induced by the roof disappears and this three profile appears the similar distribution.

Computed turbulent kinetic energy profiles for the positions at x = 25 m, 80 m, 152 m, and y = 85 m was shown in Figure 12. TKE peaks at the height of 50 m and

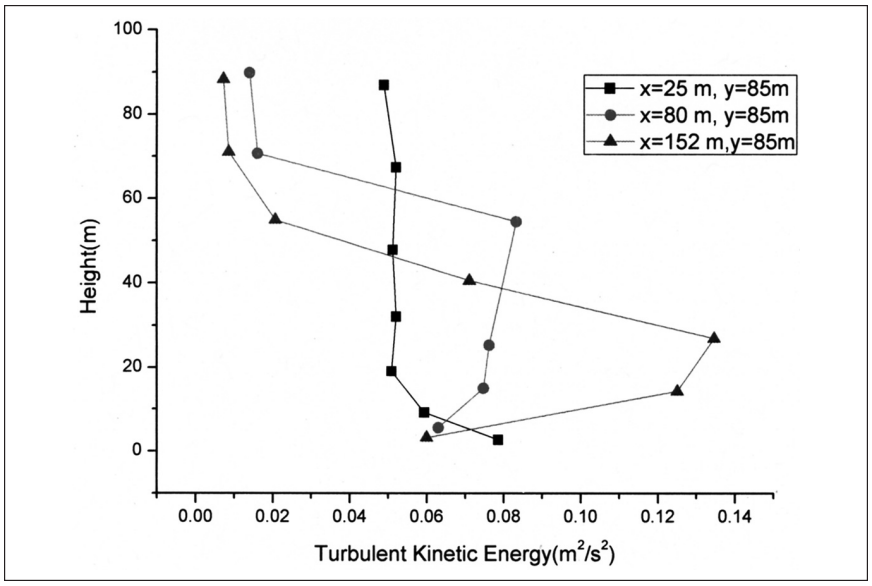

Figure 12. Turbulent kinetic energy in different height at x = 25 m, 80 m, and 152 m, y = 85 m..

30 m were presented at the profile of 80 m and 152 m. This indicates that the model can successfully simulate the region of the flow where shear stresses are dominant, such as the shear layer on the top of the canyon. It seems the same tendency of the profile of x = 80 m and 152 m from the bottom to top. But the profile of x = 25 m in front of the upwind building region indicates a different tendency that decreases with the increment of height, as the shear stresses are bottom surface.

Near the roof level, the vertical shear of horizontal wind is very strong (see Figure 11). TKE production by wind shear was a maximum near the downwind building edge because the horizontal gradient of vertical wind as well as the vertical gradient of horizontal wind is very large there. These results are the same as those of (Baik et al., 2003).

Further investigation of the x-z plane wind vector field reveals that the angle between the horizontal axis of the portal vortex and ambient wind direction varies with height. The angle is closer to being perpendicular to the ambient wind direction in the upper region than in the lower region.

Figure 13 shows that the relationship between the direction of wind speed and the height at the position of x = 25 m, 80 m, 152 m, and y = 85 m. The unit of wind speed direction is angle. It is regulated that the positive x direction and positive z direction are positive. There is no direction change (angle less than 10°)

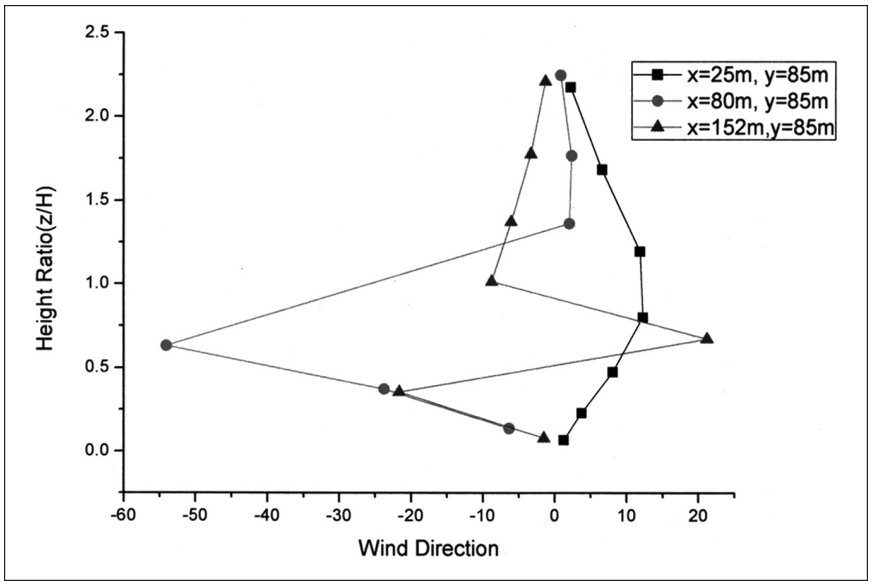

Figure 13. Wind direction indifferent height at different positions.

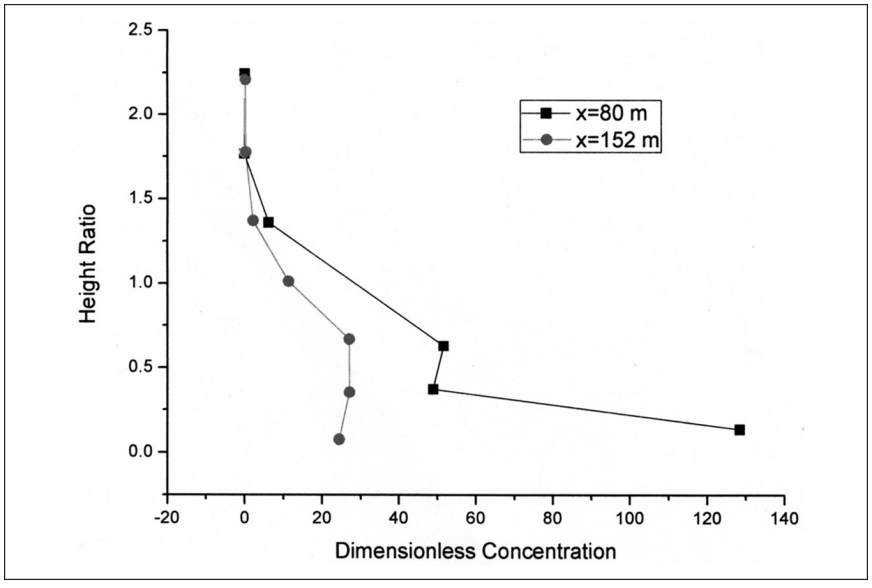

Figure 14. Dimensionless concentration at x = 80 m and 152 m.

at the position of x = 25 m, but at the position of x = 80 m and 152 m, there appears the big change in wind speed direction as the impact of vortex.

Figure 14 shows the profiles of dimensionless concentration at the position of x = 80 m and 152 m. The profile indicates that the increase of the height leads to the decrease in the concentration of the pollutant. In addition, the lowest concentration of the pollutant is zero in the higher region.

5. SUMMARY AND CONCLUSIONS

A three-dimensional CFD model with the standard k-ε turbulence model was used to investigate the effects of street canyon and area source in bottom on the wind flow and pollutant dispersion in urban street canyons using FLUENT code. The validation of the numerical model was evaluated and the model agreed with wind tunnel data.

The pollutant with the highest concentration appeared in the street canyon with the street aspect ratio of one. A vortex circulation system was produced when wind flowed normally into the canyon, which interacted with the external flow and removed contaminated air from the street canyon. The main vortex in the canyon dominated the dispersion of the pollutant and lead to the formation of the pollutant with higher concentration on the upwind or downwind building.

Pollutants emitted at the street bottom are transported to the upwind region in the lower layer of the street canyon and then transported to the upper layer of the street canyon. Therefore, the maximum pollutant concentration at any height is observed in the upwind region. Once pollutants are transported to the upper layer, some of them escape from the street canyon and others are transported into the street canyon again. The concentration is low in the downwind region where air with relatively low pollutant concentration streams into the street canyon.

The three streamline fields were simulated in x-z plane, y-z plane, and x-y plane. Through the simulation of concentration fields on the different layers and different planes, we can obtain that the pollutant concentration distribution is the same at different heights and the pollutant concentration was decreased from bottom to top, and the highest concentration was found in the corner of the down upwind building. At any height of the street canyon, the pollutant concentration is higher near the upwind building than near the downwind building. The wind speed profile data, turbulent kinetic energy profile data, wind direction profile data and dimensionless concentration profile data of position of x = 25 m, 80 m, 152 m, and y = 85 m in different heights were presented with the model simulation results. The analysis results are the same as other researchers.

Advantage of the proposed methodology is that it can be directly applied to a variety of street canyon scenarios. Further work will focus on the extension of the CFD methodology to different street configurations (aspect ratio, roof

shapes) and wind directions and turbulent kinetic energy. Finally, this methodology can be used to evaluate the concentration impact of air pollutant in complex urban canyon without considering thermal effect of bottom surface and chemical activation.

REFERENCES

Ahmadi, G., & Li, A. (2000). Computer simulation of particle transport and deposition near a small isolated building. *Journal of Industrial Aerodynamics, 84,* 23-46.

Assimakopoulos, V. D., Apsimon, H. M., & Moussiopoulos, N. (2003). A numerical study of atmospheric pollutant dispersion in different two-dimensional street canyon configurations. *Atmospheric Environment, 37,* 4037-4049.

Baik, J.-J., Kang, Y.-S., & Kim, J.-J. (2007). Modeling reactive pollutant dispersion in an urban street canyon. *Atmospheric Environment, 41,* 934-949.

Baik, J.-J., & Kim, J.-J. (1999). A numerical study of flow and pollutant dispersion characteristics in urban street canyons. *Journal of Applied Meteorology, 38,* 1576-1589.

Baik, J.-J., & Kim, J.-J. (2002). On the escape of pollutants from urban street canyons. *Atmospheric Environment, 36,* 527-536.

Baik, J.-J., Kim, J.-J., & Fernando, H. J. S. (2003). A CFD model for simulating urban flow and dispersion. *Journal of Applied Meteorology, 42,* 1636-1648.

Chan, T. L., Dong, G., Leung, C. W, Cheung, C. S., & Hung, W. T. (2002). Validation of a two-dimensional pollutant dispersion model in an isolated street canyon. *Atmospheric Environment, 36*(5), 861-872.

Chan, A. T., Au, W. T. W., So, E. S. P. (2003). Strategic guideline for street canyon geometry to achieve sustainable street air quality. Part II: Multiple canopies and canyons. *Atmospheric Environment, 37,* 2761-2772.

Fluent User's Guide (Vols. 1-4) (2005). Fluent Inc., Centerra Resource Park, Lebanon, NH.

Hassan, A. A., Crowther, J. M. (1998). Modeling of fluid flow and pollutant dispersion in a street canyon. *Environmental Monitoring andAssessment, 52,* 281-297.

Kim, J.-J., & Baik, J.-J. (2003). Effects of inflow turbulence intensity on flow and pollutant dispersion in an urban street canyon. *Journal of Wind Engineering and Industrial Aerodynamics, 91,* 309-329.

Kastner-Klein, P., and Fedorovich, E. A. (2001). Wind tunnel study of organized and turbulent air motions in street canyons. *Journal of Wind Engineering and Industrial Aerodynamics, 89*, 849-861.

Kim, J.-J., & Baik, J.-J. (2004). A numerical study of the effects of ambient wind direction on flow and dispersion in urban street canyons using the RNG k-ε turbulence model. *Atmospheric Environment, 38,* 3039-3048.

Koutsourakis, N., Neofytou, P., Venetsanos, A. G., & Bartzis, J. G. (2005). Parametric study of the dispersion aspects in a street-canyon area. *International Journal of Environment and Pollution, 25,* 155-163.

Leitl, B. M., & Meroney, R. N. (1997). Car exhaust dispersion in a streetcanyon:numerical critique of a wind tunnel experiment. *Journal of Wind Engineering and Industrial Aerodynamics, 67, 68,* 293-304.

Mensink, C., Lewyckyj, N., & Janssen, L. (2002). A new concept for air quality modeling in street canyons. *Water, Air and Soil Pollution: Focus, 2,* 339-349.

Meroney, R. N., Pavageau, M., Rafailidis, S., & Schatzmann, M. (1996). Study of line source characteristics for 2-D physical modeling of pollutant dispersion in street canyons. *Journal of Wind Engineering and Industrial Aerodynamics, 62*, 37-56.

Neofytou, P., Venetsanos, A. G., Rafailidis, S., & Bartzis, J. G. (2006). Numerical investigation of the pollution dispersion in an urban street canyon. *Environmental Modeling and Software, 21,* 525-531.

Park, Y.-S., & Baik, J.-J. (2008). Analytical solution of the advection-diffusion equation for a ground-level finite area source. *Atmospheric Environment, 42,* 9063-9069.

Patankar, S. V. (1980). *Numerical heat transfer and fluid flow*. McGraw-Hill, New York.

Ryu, Y.-H., & Baik, J.-J. (2009). Flow and dispersion in an urban cubical cavity. *Atmospheric Environment, 43,* 1721-1729.

Sahm, P., Louka, P., Ketzel, M., Guillouteau, E., & Sini, J.-F. (2002). Intercomparison of numerical urban dispersion models. Part I: Street canyon and single building configurations. *Water, Air and Soil Pollution: Focus, 2,* 587-601.

Xie, X., Huang, Z., & Wang, J.-S. (2005). Impact of building configuration on air quality in street canyon. *Atmospheric Environment, 39,* 4519-4530.

Yassin, M. F., Kellnerova, R., & Janour, Z. (2009). Impact of street intersections on air quality in an urban environment. *Atmospheric Environment, 43,* 1721-1729.

Direct reprint requests to:

Peng Wang
No. 2 Neng Yuan Road
Wushan, Guangzhou, 510640
P.R. China
e-mail: wangpeng@ms.giec.ac.cn